Determining the Neutrino Mass Hierarchy with Atmospheric Neutrinos

S. T. Petcov[a] **and T. Schwetz**[b]

Scuola Internazionale Superiore di Studi Avanzati
Via Beirut 2–4, I-34014 Trieste, Italy

Abstract

The possibility to determine the type of neutrino mass hierarchy by studying atmospheric neutrino oscillations with a detector capable to distinguish between neutrino and antineutrino events, such as magnetized iron calorimeters, is considered. We discuss how the ability to distinguish between the neutrino mass spectrum with normal and inverted hierarchy depends on detector characteristics like neutrino energy and direction resolutions or charge miss-identification, and on the systematical uncertainties related to the atmospheric neutrino fluxes. We show also how the neutrino mass hierarchy determination depends on the true values of θ_{13} and θ_{23}, as well as on the type of the true hierarchy. We find that for μ-like events, an accurate reconstruction of the energy and direction of the neutrino greatly improves the sensitivity to the type of neutrino mass spectrum. For $\sin^2 2\theta_{13} \cong 0.1$ and a precision of 5% in the reconstruction of the neutrino energy and $5°$ in the neutrino direction, the type of neutrino mass hierarchy can be identified at the 2σ C.L. with approximately 200 events. For resolutions of 15% for the neutrino energy and $15°$ for the neutrino direction roughly one order of magnitude larger event numbers are required. For a detector capable to distinguish between ν_e and $\bar{\nu}_e$ induced events the requirements on energy and direction resolutions are, in general, less demanding than for a detector with muon charge identification.

[a]Also at: Institute of Nuclear Research and Nuclear Energy, Bulgarian Academy of Sciences, 1784 Sofia, Bulgaria. Email: petcov@he.sissa.it
[b]Email: schwetz@sissa.it

1 Introduction

There has been a remarkable progress in the studies of neutrino oscillations in the last several years. The experiments with solar, atmospheric and reactor neutrinos [1–5] have provided compelling evidences for existence of neutrino oscillations driven by nonzero neutrino masses and neutrino mixing. Evidences for oscillations of neutrinos were obtained also in the first long-baseline accelerator neutrino experiment K2K [6]. The interpretation of the solar and atmospheric neutrino, and of KamLAND data in terms of neutrino oscillations requires the presence of 3-neutrino mixing in the weak charged lepton current (see, *e.g.*, [7]):

$$\nu_{l\mathrm{L}} = \sum_{j=1}^{3} U_{lj}\, \nu_{j\mathrm{L}}\,, \qquad l = e, \mu, \tau\,. \tag{1}$$

Here, $\nu_{l\mathrm{L}}$ are the three left-handed flavor neutrino fields, $\nu_{j\mathrm{L}}$ is the left-handed field of the neutrino ν_j with the mass m_j and U is the Pontecorvo-Maki-Nakagawa-Sakata (PMNS) neutrino mixing matrix [8],

$$U = \begin{pmatrix} U_{e1} & U_{e2} & U_{e3} \\ U_{\mu 1} & U_{\mu 2} & U_{\mu 3} \\ U_{\tau 1} & U_{\tau 2} & U_{\tau 3} \end{pmatrix} = \begin{pmatrix} c_{12}c_{13} & s_{12}c_{13} & s_{13}e^{-i\delta} \\ -s_{12}c_{23}-c_{12}s_{23}s_{13}e^{i\delta} & c_{12}c_{23}-s_{12}s_{23}s_{13}e^{i\delta} & s_{23}c_{13} \\ s_{12}s_{23}-c_{12}c_{23}s_{13}e^{i\delta} & -c_{12}s_{23}-s_{12}c_{23}s_{13}e^{i\delta} & c_{23}c_{13} \end{pmatrix} \tag{2}$$

where we have used a standard parametrization of U with the usual notations, $s_{ij} \equiv \sin\theta_{ij}$, $c_{ij} \equiv \cos\theta_{ij}$, and δ is the Dirac CP-violation phase [1]. If one identifies $\Delta m_{21}^2 > 0$ and Δm_{31}^2 (or Δm_{32}^2) with the neutrino mass squared differences which drive the solar and atmospheric neutrino oscillations, θ_{12} and θ_{23} represent the solar and atmospheric neutrino mixing angles, while θ_{13} is the angle limited by the data from the CHOOZ and Palo Verde experiments [12]. It follows from the data that $|\Delta m_{31(2)}^2| \gg \Delta m_{21}^2$. In this case, obviously, $\Delta m_{31}^2 \cong \Delta m_{32}^2$.

The existing solar and reactor neutrino oscillation data allow us to determine Δm_{21}^2 and $\sin^2\theta_{12}$ with a relatively good precision and to obtain rather stringent limits on $\sin^2\theta_{13}$ (see, *e.g.*, [2–5, 13–15]). The best fit values and the 99.73% C.L. allowed ranges of Δm_{21}^2 and $\sin^2\theta_{12}$ are given by [2]:

$$\Delta m_{21}^2 = 8.0 \times 10^{-5}\ \mathrm{eV}^2, \quad \sin^2\theta_{12} = 0.31\,,$$
$$\Delta m_{21}^2 = (7.1 - 9.0) \times 10^{-5}\ \mathrm{eV}^2, \quad \sin^2\theta_{12} = (0.24 - 0.40)\,, \tag{3}$$

It follows from a combined 3-ν oscillation analysis of the solar neutrino, KamLAND and CHOOZ data that [13, 15]

$$\sin^2\theta_{13} < 0.044 \quad \text{at 99.73\% C.L.} \tag{4}$$

Existing atmospheric neutrino data are essentially insensitive to θ_{13} obeying the CHOOZ limit. The Super-Kamiokande and K2K experimental results are best described in terms of

---

[1]We have not written explicitly the two possible Majorana CP-violation phases [9,10] which do not enter into the expressions for the oscillation probabilities of interest [9,11].

[2]The data imply, in particular, that maximal solar neutrino mixing is ruled out at $\sim 6\sigma$. At 95% C.L. one finds $\cos 2\theta_\odot \geq 0.26$ [13], which has important implications [16].

dominant $\nu_\mu \to \nu_\tau$ ($\bar{\nu}_\mu \to \bar{\nu}_\tau$) vacuum oscillations. The best fit values and the 99.73% C.L. allowed ranges of the atmospheric neutrino oscillation parameters read [15]:

$$|\Delta m_{31}^2| = 2.2 \times 10^{-3} \text{ eV}^2, \qquad \sin^2\theta_{23} = 0.50 \ ,$$
$$|\Delta m_{31}^2| = (1.4 - 3.3) \times 10^{-3}\text{eV}^2, \qquad \sin^2\theta_{23} = (0.34 - 0.68) \ . \tag{5}$$

The sign of Δm_{31}^2 and of $\cos 2\theta_{23}$ if $\sin^2 2\theta_{23} < 1.0$ cannot be determined using the existing data. The two possibilities, $\Delta m_{31}^2 > 0$ or $\Delta m_{31}^2 < 0$, correspond to two different types of neutrino mass spectrum: with normal hierarchy (NH), $m_1 < m_2 < m_3$, and with inverted hierarchy (IH), $m_3 < m_1 < m_2$. The fact that the sign of $\cos 2\theta_{23}$ is not determined when $\sin^2 2\theta_{23} < 1.0$ implies that if, e.g., $\sin^2 2\theta_{23} = 0.92$, two values of $\sin^2\theta_{23}$ are possible, $\sin^2\theta_{23} \cong 0.64$ or 0.36.

The neutrino oscillation parameters Δm_{21}^2, $\sin^2\theta_{12}$, $|\Delta m_{31}^2|$ and $\sin^2\theta_{23}$ are determined by the existing data with a 3σ error of approximately 12%, 27%, 50% and 34%, respectively. These parameters can (and very likely will) be measured with much higher accuracy in the future (see, e.g., [7,15,17]). The MINOS experiment [18], which collects data at present, will reduce considerably (approximately by a factor of 3) the current uncertainty in the value of $|\Delta m_{31}^2|$. The highest precision in the determination of $|\Delta m_{31}^2|$ is expected to be achieved from the studies of ν_μ-oscillations in the T2K experiment with the Super-Kamiokande detector [19]: if the true $|\Delta m_{31}^2| = 2 \times 10^{-3}$ eV^2 (and true $\sin^2\theta_{23} = 0.5$), the 3σ uncertainty in $|\Delta m_{31}^2|$ is estimated to be reduced in this experiment to $\sim 12\%$ [17]. The error diminishes with increasing of $|\Delta m_{31}^2|$. The T2K experiment will measure also $\sin^2\theta_{23}$ with an error of approximately 14% at 2σ [15]. However, this experiment would not be able to resolve the θ_{23}–$(\pi/2 - \theta_{23})$ ambiguity if $\sin^2 2\theta_{23} < 1$. In what regards the CHOOZ angle θ_{13}, there are several proposals for reactor $\bar{\nu}_e$ experiments with baseline $L \sim$ (1–2) km [20,21], which could improve the current limit by a factor of (5–10). The reactor θ_{13} experiments can compete in sensitivity with accelerator experiments T2K [19], NOνA [22] (see, e.g., [17]), and can be done on a relatively short time scale. The most precise measurement of Δm_{21}^2 could be achieved [23] using Super-Kamiokande doped with 0.1% of gadolinium (SK-Gd) for detection of reactor $\bar{\nu}_e$ [24]: getting the same flux of reactor $\bar{\nu}_e$ as KamLAND, the SK-Gd detector will have approximately a 43 times bigger reactor $\bar{\nu}_e$ event rate than KamLAND. After 3 years of data-taking with SK-Gd, Δm_{21}^2 could be determined with an error of 3.5% at 3σ [23]. A dedicated reactor $\bar{\nu}_e$ experiment with a baseline $L \sim 60$ km, tuned to the minimum of the $\bar{\nu}_e$ survival probability, could provide the most precise determination of $\sin^2\theta_{12}$ [25,26]: with statistics of ~ 60 GW ktyr and a systematic error of 2% (5%), $\sin^2\theta_{12}$ could be measured with an error of 6% (9%) at 3σ [25].

Getting more precise information about the value of the mixing angle θ_{13}, and measuring the values of Δm_{21}^2, $|\Delta m_{31}^2|$, $\sin^2\theta_{12}$ and $\sin^2\theta_{23}$ with a higher precision, is crucial for the future progress in the studies of neutrino mixing (see, e.g., [7] and the references quoted therein). Here we focus in particular on the question whether the neutrino mass spectrum is with normal or inverted hierarchy, i.e., the sign of Δm_{31}^2, which is of fundamental importance for the understanding of the origin of neutrino masses and mixing. Information on sign(Δm_{31}^2) can be obtained through matter effects in long-baseline experiments [22,27,28], or maybe from supernova neutrinos [29]. If neutrinos with definite mass are Majorana particles, information about sgn(Δm_{31}^2) could be obtained also by measuring the effective Majorana mass in neutrinoless double β-decay experiments [16,30].

In the present article we investigate in detail the possibility to obtain information on the sign of Δm_{31}^2 using the data on atmospheric neutrinos, which can be obtained in experiments with detectors able to measure the charge of the muon produced in the charged current reaction by atmospheric ν_μ or $\bar{\nu}_\mu$. Thus, in contrast to water-Čerenkov detectors, in these experiments it will be possible to distinguish between the ν_μ and $\bar{\nu}_\mu$ induced events. Among the operating detectors, MINOS has muon charge identification capabilities for multi-GeV muons [18]. The MINOS experiment is currently collecting atmospheric neutrino data. The detector has a relatively small mass, but after 5 years of data-taking it is expected to collect about 440 atmospheric ν_μ and about 260 atmospheric $\bar{\nu}_\mu$ multi-GeV events. The ATLAS and CMS experiments under preparation at the LHC accelerator at CERN will have efficient muon charge identification for multi-GeV muons and, in principle, can also be used for studies of atmospheric neutrino oscillations in the periods when the LHC accelerator will not be operational [3]. There are also plans to build a 30–50 kton magnetized iron tracking calorimeter detector in India within the India-based Neutrino Observatory (INO) project [31]. The INO detector will be based on MONOLITH design [32]. The primary goal is to study the oscillations of atmospheric ν_μ and $\bar{\nu}_\mu$. This detector is planned to have efficient muon charge identification, high muon energy resolution ($\sim 5\%$) and a muon energy threshold of about 2 GeV. It will accumulate sufficiently high statistics of atmospheric ν_μ and $\bar{\nu}_\mu$ induced events in several years, which would permit to perform a high precision study of the ν_μ and $\bar{\nu}_\mu$ disappearance due to oscillations and to search for effects of the sub-dominant $\nu_\mu \rightarrow \nu_e$ ($\nu_e \rightarrow \nu_\mu$) and $\bar{\nu}_\mu \rightarrow \bar{\nu}_e$ ($\bar{\nu}_e \rightarrow \bar{\nu}_\mu$) transitions. We consider a detector which permits to reconstruct the initial ν_μ ($\bar{\nu}_\mu$) energy and direction with a relatively good precision. The magnetized iron detectors can have such capabilities. We present results also for detectors permitting to study the oscillations of the atmospheric multi-GeV ν_e and $\bar{\nu}_e$ under similar conditions.

The possibility to obtain information about the type of neutrino mass spectrum, *i.e.*, about the sgn(Δm_{31}^2), by investigating atmospheric neutrino oscillations is based on the prediction that in the case of 3-neutrino oscillations, the Earth matter affects in a different way the transitions of neutrinos and antineutrinos [33–35]. For $\Delta m_{31}^2 > 0$, the $\nu_\mu \rightarrow \nu_e$ ($\nu_e \rightarrow \nu_\mu$) transitions of the multi-GeV neutrinos are amplified, while the transitions of antineutrinos $\bar{\nu}_\mu \rightarrow \bar{\nu}_e$ ($\bar{\nu}_e \rightarrow \bar{\nu}_\mu$) are suppressed. If $\Delta m_{31}^2 < 0$, the indicated transitions of neutrinos are suppressed and those of antineutrinos are enhanced. The magnitude of the Earth matter effects in the oscillations of multi-GeV atmospheric ν_μ ($\bar{\nu}_\mu$) and ν_e ($\bar{\nu}_e$) depends critically on the value of $\sin^2 \theta_{13}$: the effects can be substantial for $\sin^2 \theta_{13} \gtrsim 0.01$; for $\sin^2 \theta_{13} \ll 0.01$ they are exceedingly small. The difference between the oscillations of neutrinos and antineutrinos can be relatively large and observable in the samples of $\mu^\pm$ events with $E_\mu \sim (2-10)$ GeV, from atmospheric ν's with a large path length in the Earth, crossing deeply the Earth mantle [27] or the mantle and the core [36–40]. These are the neutrinos for which $\cos\theta_n \gtrsim (0.3 - 0.4)$, where θ_n is the Nadir angle characterizing the neutrino trajectory in the Earth.

Let us note that three-flavour effects in atmospheric neutrino oscillations including the Earth matter effects have been widely studied in the literature; for an incomplete list see [40–55]. A rather detailed analysis for the MONOLITH detector has been performed in [52], and magnetized iron detectors in general have been considered previously in [42, 53–55]. A large

---

[3]We thank F. Vannucci for pointing out this possibility to us.

number of studies have been done for water-Čerenkov detectors [41, 47–51]. Such detectors have a more limited sensitivity to the type of neutrino mass hierarchy, because only the sum of neutrino and antineutrino induced events can be observed. Since large matter effects occur for neutrino if $\Delta m_{31}^2 > 0$ and for antineutrinos if $\Delta m_{31}^2 < 0$, summing the corresponding events significantly diminishes the effect of changing the sign of Δm_{31}^2. The remaining sensitivity (see *e.g.*, [41, 50]) is due to the facts that neutrino and antineutrino cross sections differ roughly by a factor of 2, and that a huge number of events is available in mega ton scale experiments [48]. Obviously, such a "dilution" of the magnitude of the matter effects does not take place in the samples of μ^- and μ^+ events, which can be collected in the experiments with muon charge identification.

2 Three-Neutrino Oscillations of Atmospheric Neutrinos

In the present Section we will review briefly the formalism and the physics of the 3-neutrino oscillations of the multi-GeV atmospheric neutrinos with energy $E \sim (1 - 10)$ GeV in the Earth (see, *e.g.*, [41] and the references quoted therein for further details). The probabilities of the flavour neutrino oscillations in matter of interest, $\nu_\alpha \to \nu_\beta$, $\bar\nu_\alpha \to \bar\nu_\beta$, $\alpha = e, \mu$, $\beta = e, \mu, \tau$, can be written for an arbitrary matter density profile as

$$P_{\alpha\beta}^p = |A_{\alpha\beta}^p|^2, \qquad (6)$$

where $A_{\alpha\beta}^p$ is the probability amplitude which is obtained by solving a Schrödinger-like system of coupled evolution equations and $p = \nu\ (\bar\nu)$ for neutrinos (antineutrinos). We use the standard parameterization of the PMNS mixing matrix [56], $U = O_{23} U_\delta O_{13} O_{12}$, where O_{ij} is the orthogonal matrix of rotations in the ij-plane which depends on the mixing angle θ_{ij}, and $U_\delta = \mathrm{diag}(1, 1, e^{i\delta})$, δ being the Dirac CP-violating phase. Exploiting the fact that the matrix $O_{23} U_\delta$ commutes with the matrix containing the matter potential, it is easy to show that [57] without loss of generality $A_{\alpha\beta}^p$ can be written as

$$A^p = O_{23} U_\delta A'^p U_\delta^\dagger O_{23}^T, \qquad (7)$$

where A'^p does not depend on θ_{23} and δ. We adopt further the approximation of setting the neutrino mass-squared difference Δm_{21}^2, responsible for the solar neutrino oscillations, to zero [4]. In this approximation the probabilities of interest are independent of the mixing angle θ_{12} and the Dirac CP-violating phase δ. Moreover, the calculation of A'^p is reduced effectively to the calculation of probability amplitudes in the case of two neutrino mixing [57]. For neutrinos with energy E and crossing the Earth along a trajectory characterized by a Nadir angle θ_n, the probability of the 2-neutrino $\nu_e \to \nu'\ (\bar\nu_e \to \bar\nu')$ transitions is given by

$$P^{2p} \equiv P^{2p}(\Delta m_{31}^2, \theta_{13}; E, \theta_n) \equiv |A_{13}'^p|^2 = |A_{31}'^p|^2 = 1 - |A_{11}'^p|^2 = 1 - |A_{33}'^p|^2, \qquad (8)$$

where $p = \nu\ (\bar\nu)$, and $\nu' = s_{23} \nu_\mu + c_{23} \nu_\tau$ [57]. The three-neutrino oscillation probabilities are

---

[4] This can be justified by the fact that we are interested in oscillations of multi-GeV (atmospheric) neutrinos in the Earth and that the existing data implies $\Delta m_{21}^2 / |\Delta m_{31}^2| \cong 0.04 \ll 1$. We have checked by explicit calculations that for the energy range of interest, $E_\nu \gtrsim 1$ GeV, our results are not affected by setting $\Delta m_{21}^2 = 0$ if Δm_{21}^2 has values in the interval given in Eq. (3).

obtained as

$$P_{ee}^{3p} \cong |A_{11}'^p|^2 = 1 - P^{2p}, \tag{9}$$

$$P_{\mu e}^{3p} = P_{e\mu}^{3p} \cong s_{23}^2 |A_{13}'^p|^2 = s_{23}^2 P^{2p}, \tag{10}$$

$$P_{e\tau}^{3p} \cong c_{23}^2 |A_{13}'^p|^2 = c_{23}^2 P^{2p}, \tag{11}$$

$$P_{\mu\mu}^{3p} \cong c_{23}^4 + s_{23}^4 |A_{33}'^p|^2 + 2c_{23}^2 s_{23}^2 \operatorname{Re}(A_{33}'^p) \tag{12}$$

$$= 1 - s_{23}^4 P^{2p} - 2c_{23}^2 s_{23}^2 \left[1 - \operatorname{Re}(e^{-i\kappa_p} A_{\nu'\nu'}^{2p})\right], \tag{13}$$

$$P_{\mu\tau}^{3p} = 1 - P_{\mu\mu}^{3p} - P_{\mu e}^{3p}. \tag{14}$$

In Eq. (13) we used $e^{-i\kappa_p} A_{\nu'\nu'}^{2p} \equiv A_{33}'^p$, where κ_p and $A_{\nu'\nu'}^{2p}$ are a known phase and 2-neutrino transition probability amplitude [36, 37, 57].

The fluxes of atmospheric $\nu_{e,\mu}$ and $\bar\nu_{e,\mu}$ of energy E, which reach the detector after crossing the Earth along a given trajectory specified by the value of θ_n are given by the following expressions in the case of the 3-neutrino oscillations under discussion [37]:

$$\bar\Phi_e^p(E, \theta_n) \cong \Phi_e^p \left[1 + (s_{23}^2 r^p - 1) P^{2p}\right], \tag{15}$$

$$\bar\Phi_\mu^p(E, \theta_n) \cong \Phi_\mu^p \left\{1 + s_{23}^4 [(s_{23}^2 r^p)^{-1} - 1] P^{2p} - 2c_{23}^2 s_{23}^2 \left[1 - \operatorname{Re}(A_{33}'^p)\right]\right\}, \tag{16}$$

where $\Phi_{e(\mu)}^p = \Phi_{e(\mu)}^p(E, \theta_n)$ are the $\nu_{e(\mu)}$ ($p = \nu$) and $\bar\nu_{e(\mu)}$ ($p = \bar\nu$) fluxes in the absence of neutrino oscillations, and

$$r^p \equiv r^p(E, \theta_n) \equiv \frac{\Phi_\mu^p(E, \theta_n)}{\Phi_e^p(E, \theta_n)}. \tag{17}$$

The interpretation of the SK atmospheric neutrino data in terms of dominant $\nu_\mu \to \nu_\tau$ and $\bar\nu_\mu \to \bar\nu_\tau$ oscillations requires the parameter s_{23}^2 to lie approximately in the interval $(0.30-0.70)$, with 0.5 being the statistically preferred value. For the predicted ratio $r^p(E, \theta_n)$ of the fluxes of atmospheric ν_μ ($\bar\nu_\mu$) and ν_e ($\bar\nu_e$) with energy $E \cong (2-10)$ GeV, crossing the Earth along trajectories for which $0.3 \lesssim \cos\theta_n \leq 1.0$, one has [58]: $r^p(E, \theta_n) \cong (2.6-4.5)$. Correspondingly, for $s_{23}^2 = 0.5$ (0.64) we find for the factors multiplying the 2-neutrino transition probability P^{2p} in Eqs. (15) and (16): $(s_{23}^2 r^p - 1) \cong 0.3 - 1.3$ $(0.66 - 1.9)$, and $s_{23}^4 [1 - (s_{23}^2 r^p)^{-1}] \cong 0.06 - 0.14$ $(0.16 - 0.27)$. This result implies that the 2-neutrino transition probability P^{2p} can have a much larger effect on the flux of atmospheric ν_e ($\bar\nu_e$) than on the flux of atmospheric ν_μ ($\bar\nu_\mu$).

In our further analysis performed in Sections 5 and 6, the matrix A' and correspondingly the probabilities P^{2p} and the amplitudes $A_{33}'^p = e^{-i\kappa_p} A_{\nu'\nu'}^{2p}$, are obtained by solving the relevant system of evolution equations (see, e.g., [57]) numerically using a realistic Earth density profile provided by the PREM model [59]. As is well-known, the Earth density distribution in the existing Earth models is assumed to be spherically symmetric. There are two major density structures—the core and the mantle, and a certain number of substructures (shells or layers) [5]. The mean electron number densities in the mantle and in the core read [59]: $\bar N_e^{man} \cong 2.2\ N_A\,\mathrm{cm}^{-3}$, $\bar N_e^c \cong 5.4\ N_A\,\mathrm{cm}^{-3}$, N_A being the Avogadro number.

---

[5]According to the Earth models [59, 60], the core has a radius $R_c = 3485.7$ km, the Earth mantle depth is approximately $R_{man} = 2885.3$ km, and the Earth radius is $R_\oplus = 6371$ km. The mean values of the matter densities and the electron fraction numbers in the mantle and in the core read, respectively: $\bar\rho_{man} \cong 4.5$ g/cm^3, $\bar\rho_c \cong 11.5$ g/cm^3, and [61] $Y_e^{man} = 0.49$, $Y_e^c = 0.467$.

Rather simple analytic expressions for the quantities of interest, P^{2p}, κ_p and $A^{2p}_{\nu'\nu'}$ have been derived in the two-layer model of the Earth density distribution (see, *e.g.*, [56]). In this model the electron number densities in the mantle and in the core are assumed to be constant [6]. For the atmospheric neutrinos crossing only the Earth mantle but not the Earth core ($\theta_n \gtrsim 33.17°$), for instance, the expressions for P^{2p}, κ_p and $A^{2p}_{\nu'\nu'}$ in the two-layer model are given by (see, *e.g.*, [41]):

$$P^{2p} = \sin^2\left(\frac{\Delta E'^p_m L}{2}\right) \sin^2 2\theta'^p_m, \tag{18}$$

$$\kappa_{\nu(\bar\nu)} \cong \frac{1}{2}\left[\frac{\Delta m^2_{31} L}{2E} \genfrac{}{}{0pt}{}{+}{(-)} \sqrt{2} G_F \bar N^{man}_e L - \Delta E'^{\nu(\bar\nu)}_m L\right], \tag{19}$$

$$A^{2p}_{\nu'\nu'} = 1 + \left(e^{-i\Delta E'^p_m L} - 1\right)\cos^2 \theta'^p_m. \tag{20}$$

Here $\Delta E'^p_m$ and θ'^p_m are the difference between the energies of the two matter-eigenstate neutrinos and the mixing angle (in matter) in the mantle, which coincide with $\Delta m^2_{31}/(2E)$ and θ_{13} in vacuum, and L is the distance the neutrino travels in the mantle, $L = 2R_\oplus \cos\theta_n$, where $R_\oplus = 6371$ km is the Earth radius. Similar expressions have been derived in the case of neutrinos crossing the Earth core [36, 37] (see also [41]).

For a given neutrino trajectory in the Earth, the 2-neutrino transition probability P^{2p} is a rather slowly varying function of the neutrino energy in the interval of interest $E \sim (1 - 10)$ GeV. In contrast, the interference term $\mathrm{Re}(e^{-i\kappa_p} A^{2p}_{\nu'\nu'})$ in the expression of the ν_μ ($\bar\nu_\mu$) survival probability $P^{3p}_{\mu\mu}$ is a relatively fast oscillating function of E. As a consequence, the integration over the atmospheric neutrino energy in the indicated interval does not affect significantly the probability P^{2p}, while it tends to suppress strongly the effects due to the term $\mathrm{Re}(e^{-i\kappa_p} A^{2p}_{\nu'\nu'})$. The specific properties of the oscillating term $\mathrm{Re}(e^{-i\kappa_p} A^{2p}_{\nu'\nu'})$, present in the expression of the ν_μ ($\bar\nu_\mu$) survival probability $P^{3p}_{\mu\mu}$, have been discussed in the case of neutrinos crossing only the Earth mantle in [54]. A further discussion of the interplay between the term $\propto P^{2p}$ and that $\propto \mathrm{Re}(A'^p_{33})$ in the ν_μ ($\bar\nu_\mu$) survival probability is given in Section 4.

For $\Delta m^2_{31} > 0$, we can have $P_{2\nu} \cong 1$ in the case of atmospheric neutrinos crossing only the mantle for neutrino energy and path-length given by $E_{res} \cong 6.6\,\Delta m^2_{31}[10^{-3}\text{ eV}^2]\cos 2\theta_{13} (\bar N^{man}_e[N_A\text{cm}^{-3}])^{-1}$ GeV and $L[10^4\text{ km}] \cong (0.8\ \bar N^{man}_e[N_A\text{cm}^{-3}]\tan 2\theta_{13})^{-1}$. Taking $\Delta m^2_{31} \cong 2.0 \times 10^{-3}$ eV^2 and $\sin^2\theta_{13} = 0.05$ (0.025) one finds that $E_{res} \cong 6.6$ GeV, and that we can have $P_{2\nu} \cong 1$ only if $L \cong 8000$ (10000) km.

In the case of atmospheric neutrinos crossing the Earth core, it is possible to have $P^{2\nu} \cong 1$ for $\sin^2\theta_{13} < 0.05$ and $\Delta m^2_{31} > 0$, only due to the effect of maximal constructive interference between the amplitudes of the the $\nu_e \rightarrow \nu'_\tau$ transitions in the Earth mantle and in the Earth core [36–39] [7]. The *mantle-core enhancement effect* is caused by the existence (for a given

---

[6]Numerical calculations have shown [36, 62] that, *e.g.*, the 2-neutrino oscillation probability P^{2p} of interest, calculated within the two-layer model of the Earth with $\bar N^{man}_e$ and $\bar N^c_e$ for a given neutrino trajectory determined using the PREM (or the Stacey [60]) model, reproduces with a rather high precision the corresponding probability, calculated by solving numerically the relevant system of evolution equations with the more sophisticated Earth density profile of the PREM (or Stacey) model.

[7]The effect differs from the MSW one [36] and the enhancement happens in the case of interest at a value of the energy between the resonance energies corresponding to the density in the mantle and that of the core.

ν-trajectory through the Earth core) of *points of resonance-like total neutrino conversion,* $P^{2\nu} = 1$, in the corresponding space of ν-oscillation parameters [38, 39]. The points where $P^{2\nu} = 1$ are determined by two conditions [38,39]. A rather complete set of values of $\Delta m_{31}^2/E$ and $\sin^2 2\theta_{13}$ for which both conditions hold and $P^{2\nu} = 1$ was found in [39]. The location of these points determines the regions where $P^{2\nu}$ is large, $P^{2\nu} \gtrsim 0.5$. For $\sin^2 \theta_{13} < 0.05$, there are two sets of values of Δm_{31}^2 and $\sin^2 \theta_{13}$ for which $P^{2\nu} = 1$: for, *e.g.*, $\theta_n = 0$; 13^0; 23^0, we have $P^{2\nu} = 1$ at 1) $\sin^2 2\theta_{13} = 0.034$; 0.039; 0.051, and at 2) $\sin^2 2\theta_{13} = 0.15$; 0.17; 0.22 (see Table 2 in [39]). For $\Delta m_{31}^2 = 2.0 \times 10^{-3}$ eV^2, $P^{2\nu} = 1$ occurs in the case 1) at $E \cong (2.8-3.1)$ GeV. The effects of the mantle-core enhancement of $P^{2\nu}$ (or $P^{2\bar{\nu}}$ if $\Delta m_{31}^2 < 0$) increase rapidly with $\sin^2 2\theta_{13}$ as long as $\sin^2 2\theta_{13} \lesssim 0.06$, and should exhibit a rather weak dependence on $\sin^2 2\theta_{13}$ for $0.06 \lesssim \sin^2 2\theta_{13} < 0.19$.

In our further analysis amplitudes of interest $A_{13}'^{p}$, $A_{33}'^{p}$, *etc* are obtained by solving the evolution equation numerically using a realistic Earth density profile [59]. To simplify the notation we introduce the abbreviation $\Delta m^2 \equiv \Delta m_{31}^2$.

3   Description of the Analysis

Detection cross section. In the following we assume detection of atmospheric neutrinos of flavour $\alpha = e, \mu$ by the charged-current interaction $\nu_\alpha + N \to \alpha + X$, where N is the detector nucleon, α is the charged lepton, and X contains all the additional particles in the final state. Since we are interested in energies large compared to the muon mass the total cross section for this reaction is equal for ν_e and ν_μ, and we denote it by $\sigma^p(E_\nu)$, where $p = \nu(\bar{\nu})$ for neutrinos (antineutrinos). We take into account that in realistic detectors there will be an energy threshold E_{thr} for the detection of the charged leptons (*e.g.*, muons). Therefore, the relevant cross section is given by

$$\sigma^p(E_\nu) = \int_{E_{\text{thr}}}^{E_\nu} dE_\alpha \frac{d\sigma^p}{dE_\alpha} \approx \sigma_{\text{tot}}^p(E_\nu) \left[1 - \frac{E_{\text{thr}}}{E_\nu} \left(\frac{1 + a^p E_{\text{thr}}^2/E_\nu^2}{1 + a^p} \right) \right] , \qquad (21)$$

where σ_{tot}^p is the total cross section for $E_{\text{thr}} = 0$, and $a^\nu = \bar{Q}/3Q$, $a^{\bar{\nu}} = Q/3\bar{Q}$ with $Q \approx 0.44$, $\bar{Q} \approx 0.06$ being the average fractions of the momentum of the proton carried by quarks and anti-quarks, respectively. These numbers hold for a iso-scalar target, and our results do hardly depend on the precise values adopted for Q and $\bar{Q}$. In our calculations we use a threshold of $E_{\text{thr}} = 2$ GeV. We assume that the detector provides enough information on momentum and energy of the final states, such that the initial neutrino energy and neutrino direction can be reconstructed with an accuracy of σ_E and σ_{dir}, respectively.

Atmospheric neutrino fluxes. For the initial fluxes of atmospheric neutrinos we use the results of 3-dimensional calculations [63]. Since we consider only upward-going events with $0.1 \leq \cos\theta_n \leq 1$, where θ_n is the Nadir angle of the neutrino, one can neglect the height distribution of the neutrino production in the atmosphere. Furthermore, we average the fluxes over the azimuthal angle, such that we finally obtain fluxes $\Phi_\alpha^p(E_\nu, \cos\theta_n)$, with $\alpha = e, \mu$ and $p = \nu(\bar{\nu})$.

Calculation of the event rates. Using the fluxes, cross sections and oscillation probabilities discussed earlier, the predicted spectrum of α-like events as a function of the neutrino

energy E_ν and the Nadir angle $\cos\theta_n$ can be calculated by

$$S_\alpha^p(E_\nu, \cos\theta_n) \propto \left[\Phi_\alpha^p(E_\nu, \cos\theta_n)P_{\alpha\alpha}^p(E_\nu, \cos\theta_n) + \Phi_\beta^p(E_\nu, \cos\theta_n)P_{\beta\alpha}^p(E_\nu, \cos\theta_n)\right]\sigma^p(E_\nu) \tag{22}$$

where $\alpha, \beta = e, \mu$, $\alpha \neq \beta$. To take into account the uncertainty in the reconstruction of neutrino energy and direction we fold this spectrum with Gaussian resolution functions R_E and R_{dir}:

$$\hat{S}_\alpha^p(E_\nu, \cos\theta_n) = \int dE'_\nu\, R_E(E_\nu, E'_\nu)\int d(\cos\theta'_n)\, R_{\text{dir}}(\cos\theta_n, \cos\theta'_n)\, S_\alpha^p(E'_\nu, \cos\theta'_n). \tag{23}$$

We assume a constant *relative* energy resolution, *i.e.*, $\sigma_E \propto E_\nu$. Furthermore, we adopt the approximation of an angular resolution σ_{dir} being independent of the neutrino energy. In the resolution function R_{dir} we convert σ_{dir} into an uncertainty on $\cos\theta_n$ by $\sigma(\cos\theta_n) = \sigma_{\text{dir}}\sin\theta_n$ with σ_{dir} in radiant.

Departing from the spectrum given in Eq. (23) we calculate event numbers divided into N_E^{bin} bins in E_ν between E_ν^{min} and E_ν^{max}, and into N_θ^{bin} bins in $\cos\theta_n$ between $\cos\theta_n^{\text{min}}$ and $\cos\theta_n^{\text{max}}$:

$$N_{jk}^p = \mathcal{C}\int_j dE_\nu \int_k d(\cos\theta_n)\hat{S}_\alpha^p(E_\nu, \cos\theta_n) \tag{24}$$

where the integration boundaries are given by the jth bin in neutrino energy and the kth bin in $\cos\theta_n$. The normalization constant $\mathcal{C}$ is determined by fixing the total number of neutrino and antineutrino events to N^{tot} for specified values of the oscillation parameters $\boldsymbol{x} = (\theta_{13}, \theta_{23}, \Delta m^2)$:

$$N^{\text{tot}} = \sum_{j=1}^{N_E^{\text{bin}}}\sum_{k=1}^{N_\theta^{\text{bin}}}\sum_{p=\nu,\bar\nu} N_{jk}^p(\boldsymbol{x}). \tag{25}$$

In general we choose for the normalization the "true" parameter values $\boldsymbol{x}^{\text{true}}$, the same which are used to simulate the "data" (see below). For the calculation of our actual observables we take into account that in a realistic experiment charge identification will not be perfect. Assuming that the charge assignment is correct for a fraction f_{ID} of all events we obtain the actual observables in each bin for neutrinos and antineutrinos by

$$\begin{aligned} R_{jk}^\nu &= f_{\text{ID}}\, N_{jk}^\nu + (1 - f_{\text{ID}})\, N_{jk}^{\bar\nu} \\ R_{jk}^{\bar\nu} &= f_{\text{ID}}\, N_{jk}^{\bar\nu} + (1 - f_{\text{ID}})\, N_{jk}^\nu \end{aligned} \tag{26}$$

Hence, 100% correct charge identification corresponds to $f_{\text{ID}} = 1$, and $f_{\text{ID}} = 0.5$ implies no information on the charge, since neutrino and antineutrino events are summed with equal weight. For simplicity we assume here that f_{ID} does neither depend on the energy nor on the direction.[8]

The χ^2-analysis and systematic errors. We investigate the potential to determine the mass hierarchy by performing a statistical analysis based on a χ^2-function. Following the standard approach to construct a χ-function for future experiments we calculate "data" by adopting "true values" $\boldsymbol{x}^{\text{true}}$ for the oscillation parameters:

$$D_{jk}^p = R_{jk}^p(\boldsymbol{x}^{\text{true}}). \tag{27}$$

---

[8]For a given experiment this might be only a rough approximation, since in general the ability to identify the charge of a particle *does* depend on the energy and on the direction relative to the magnetic field.

index l	systematic effect	value
1	overall normalization	20%
2	$\nu/\bar{\nu}$ ratio	5%
3	ν_μ/ν_e ratio of fluxes	5%
$4-7$	$\cos\theta_n$ dependence of fluxes	5%
$8-11$	energy dependence of fluxes	5%
12	uncertainty on f_{ID}	5%

Table 1: Systematic uncertainties included in the χ^2 analysis.

In the theoretical prediction we take into account several sources of systematic errors by introducing 12 pull variables $\boldsymbol{\xi} = (\xi_1, \ldots, \xi_{12})$:

$$T_{jk}^p(\boldsymbol{x}, \boldsymbol{\xi}) = R_{jk}^p(\boldsymbol{x}) \left(1 + \sum_{l=1}^{12} \xi_l \, \pi_{jk,l}^p \right) , \tag{28}$$

with appropriately defined "couplings" $\pi_{jk,l}^p$. In the systematic error treatment we follow closely the description given in the appendix of [64], where also a definition of the $\pi_{jk,l}^p$ can be found (see also [3]). The systematic effects included in our analysis are listed in Tab. 1. We consider a fully correlated overall normalization error from various sources like uncertainties in the atmospheric neutrino fluxes, the cross sections, the fiducial detector mass, or efficiencies. We adopt a conservative value of 20%. Furthermore, we take into account an uncertainty in the neutrino/antineutrino ratio (including fluxes as well as cross sections) and an error on the ratio of e-like to μ-like fluxes. In addition to these normalization errors we allow also for uncertainties in the *shape* of the neutrino fluxes by introducing a linear tilt in $\cos\theta_n$ and E_ν, uncorrelated between the four fluxes of $\nu_e, \bar{\nu}_e, \nu_\mu, \bar{\nu}_\mu$. And finally we take into account the effect of an uncertainty in the charge identification fraction f_{ID}. We consider the values for the systematics given in Tab. 1 as conservative estimates. We will use these representative values to illustrate the impact of such kind of uncertainties on the mass hierarchy sensitivity by comparing the χ^2 with and without including them.

Allowing for rather small event numbers per bin we adopt a χ^2-definition based on Poisson statistics:

$$\chi^2(\boldsymbol{x}^{\mathrm{true}}; \boldsymbol{x}) = \min_{\boldsymbol{\xi}} \left[2 \sum_{j=1}^{N_E^{\mathrm{bin}}} \sum_{k=1}^{N_\theta^{\mathrm{bin}}} \sum_{p=\nu,\bar{\nu}} \left(T_{jk}^p(\boldsymbol{x}, \boldsymbol{\xi}) - D_{jk}^p + D_{jk}^p \ln \frac{D_{jk}^p}{T_{jk}^p(\boldsymbol{x}, \boldsymbol{\xi})} \right) + \sum_{l=1}^{12} \xi_l^2 \right] \tag{29}$$

Since we are going to consider up to $N_E^{\mathrm{bin}} \times N_\theta^{\mathrm{bin}} = 20 \times 20$ bins, and the total number of events is expected to be of order of a few hundred, the actual number of events per bin will be often less than 1. In a real experiment of that kind an un-binned likelihood analysis should be performed in order to extract most information from the available data. In the absence of real data, however, the χ^2 procedure outlined here still describes the performance of an "average" experiment.

4 Qualitative Discussion

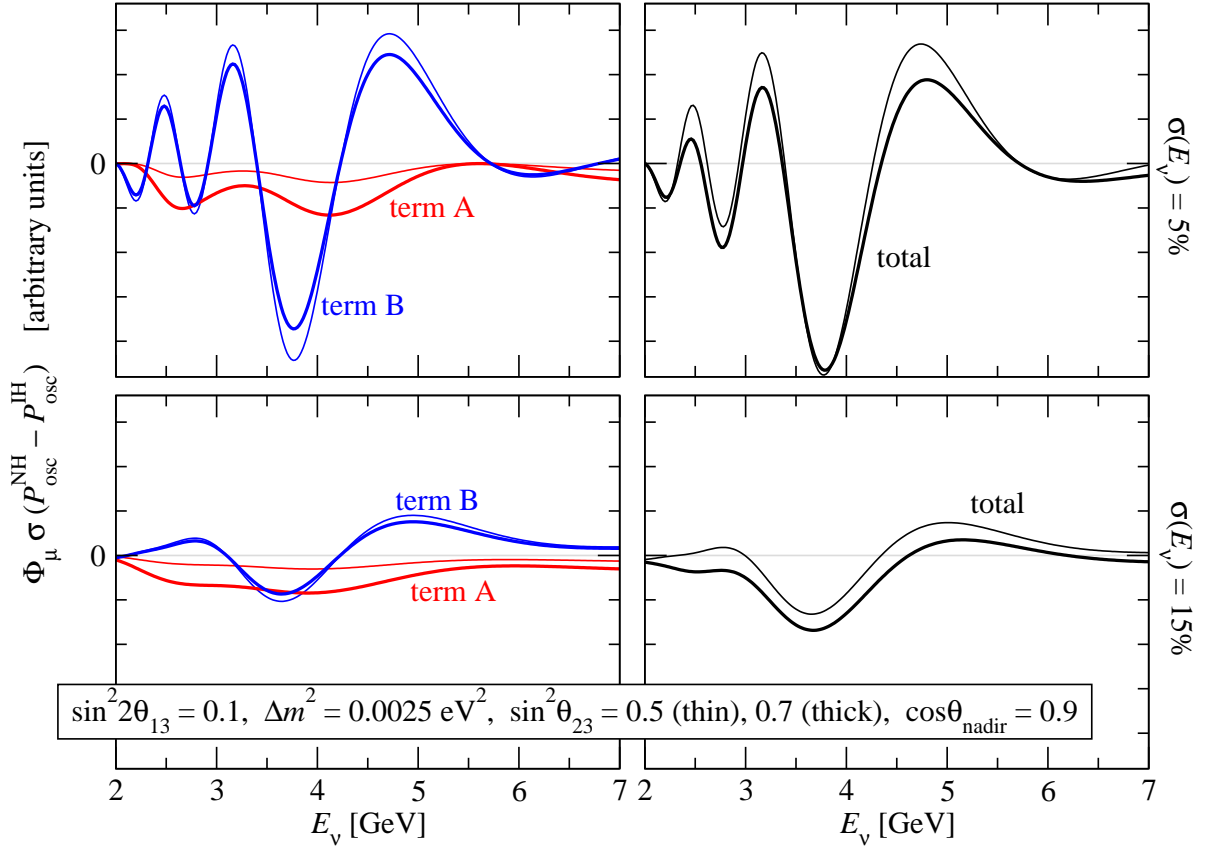In this Section we give a qualitative discussion of the effects allowing to distinguish the

10

Figure 1: The difference between the μ-like event energy spectra corresponding to $\Delta m^2 > 0$ (NH) and $\Delta m^2 < 0$ (IH), ΔS_μ^ν, defined in Eq. (32). In the left panels terms A and B are displayed separately, in the right panels the total effect is shown. In the upper (lower) panels an energy resolution of 5% (15%) is taken into account. The Nadir angle is fixed to $\cos\theta_n = 0.9$ (no smearing included). Thin (thick) curves correspond to $\sin^2\theta_{23} = 0.5\,(0.7)$.

two types of neutrino mass hierarchy under the condition of relatively precise measurement of the event spectrum. This considerations will allow to obtain some insight in the numerical results presented in the subsequent sections.

Substituting Eqs. (15) and (16) into Eq. (22), one obtains for the predicted event spectrum (see, *e.g.*, [42])

$$S_e^p \;\;\propto\;\; \Phi_e^p \sigma^p \left[1 + (r^p \sin^2\theta_{23} - 1) P_{2\nu}^p \right] \,, \tag{30}$$

$$S_\mu^p \;\;\propto\;\; \Phi_\mu^p \sigma^p \left[1 + \sin^2\theta_{23} \left(\frac{1}{r^p} - \sin^2\theta_{23} \right) P_{2\nu}^p - \frac{1}{2}\sin^2 2\theta_{23} \left(1 - \mathrm{Re}\left(A_{33}'^p \right) \right) \right] \,, \tag{31}$$

where $r^p \equiv r^p(E_\nu, \cos\theta_n)$ is defined in Eq. (17) and we have suppressed the dependence on E_ν and $\cos\theta_n$.

In order to determine the type of the neutrino mass spectrum one can explore the difference in the event energy spectra as predicted by the NH and IH. To illustrate the effect for

μ-like events, let us consider

$$\Delta S_\mu^p \propto \underbrace{\Phi_\mu^p \sigma^p \sin^2\theta_{23} \left(\frac{1}{r^p} - \sin^2\theta_{23} \right) \Delta P_{2\nu}^p}_{\text{term A}} + \underbrace{\Phi_\mu^p \sigma^p \frac{1}{2}\sin^2 2\theta_{23} \Delta \text{Re}\left(A_{33}'^p \right)}_{\text{term B}}, \qquad (32)$$

with $\Delta X \equiv X(\text{NH}) - X(\text{IH})$. In Fig. 1 we show ΔS_μ^ν, where in the left panels we display the two terms in Eq. (32) separately, whereas the right panels show the total effect, *i.e.*, the sum of "term A" and "term B". In this plot we take into account also the effect of the finite energy resolution, *i.e.*, we average ΔS_μ^ν according to Eq. (23) assuming $\sigma_E = 5\%\,(15\%)$ for the upper (lower) panels. Note however, that we do not average over the Nadir angle, and we fix $\cos\theta_n = 0.9$.

From the upper left panel we observe that term B provides a large signal with a fast oscillatory behaviour in neutrino energy. In contrast, term A is much less sensitive to the neutrino energy, in particular its sign does not change. This implies that the averaging implied by worse energy resolutions mainly affects term B, whereas term A is rather insensitive to it. This effect can be observed in the lower left panel, where the signal from term B is significantly reduced with respect to the upper panel, but the size of term A is similar. As visible in the right panels, the total signal is also strongly affected by the energy averaging, since for good resolutions term B dominates. We find a qualitatively similar behaviour also for other values of the Nadir angle, as well as for the distribution in $\cos\theta_n$ for fixed energy, and for antineutrinos.

Furthermore, we illustrate in Fig. 1 the dependence of the hierarchy effect on θ_{23}. According to Eq. (32), for term A this dependence is controlled by the factor $\sin^2\theta_{23}(1/r^p - \sin^2\theta_{23})$, where in the relevant range of energies $r^p \simeq 2.6 - 4.5$. Hence, term A increases with $\sin^2\theta_{23}$, very similar to effects in e-like events (see, *e.g.*, [41] for a detailed discussion). In contrast, term B depends on $\sin^2 2\theta_{23}$, and therefore it has a maximum for $\theta_{23} = \pi/4$. This behaviour of terms A and B is visible in the left panels of Fig. 1. The dependence of the total effect on θ_{23} emerges from a non-trivial interplay of the two terms, where the effect of averaging plays a crucial role to control the relative size of them. We will return to this discussion in Sec. 6, where we present the dependence of the hierarchy sensitivity as a function of $\sin^2\theta_{23}$.

5   Energy and Angular Resolution, Number of Bins, Charge ID, and Systematics

In this Section we discuss in some detail the impact of "experimental" parameters such as energy and angular resolution, the number of bins used in the analysis, charge identification, and systematical errors on the ability to identify the neutrino mass hierarchy. Since our aim in this section is to identify the impact of these parameters on the sensitivity we perform a simplified analysis. For most purposes we take into account only statistical errors, *i.e.* we fix all the pull parameters $\boldsymbol{\xi}$ in Eq. (29) to zero. Furthermore, we compare NH and IH for *fixed* oscillation parameters. More precisely, we calculate data for the NH and the true values $\boldsymbol{x}^{\text{true}} = \boldsymbol{x}^{\text{NH}} = (\theta_{13}, \theta_{23}, \Delta m^2)$ with $\Delta m^2 > 0$. Then the χ^2 is calculated for the *same* oscillation parameters but for IH:

$$\Delta\chi^2(\text{NH};\text{IH}) \equiv \chi^2(\boldsymbol{x}^{\text{NH}}; \boldsymbol{x}^{\text{IH}}) \qquad (33)$$
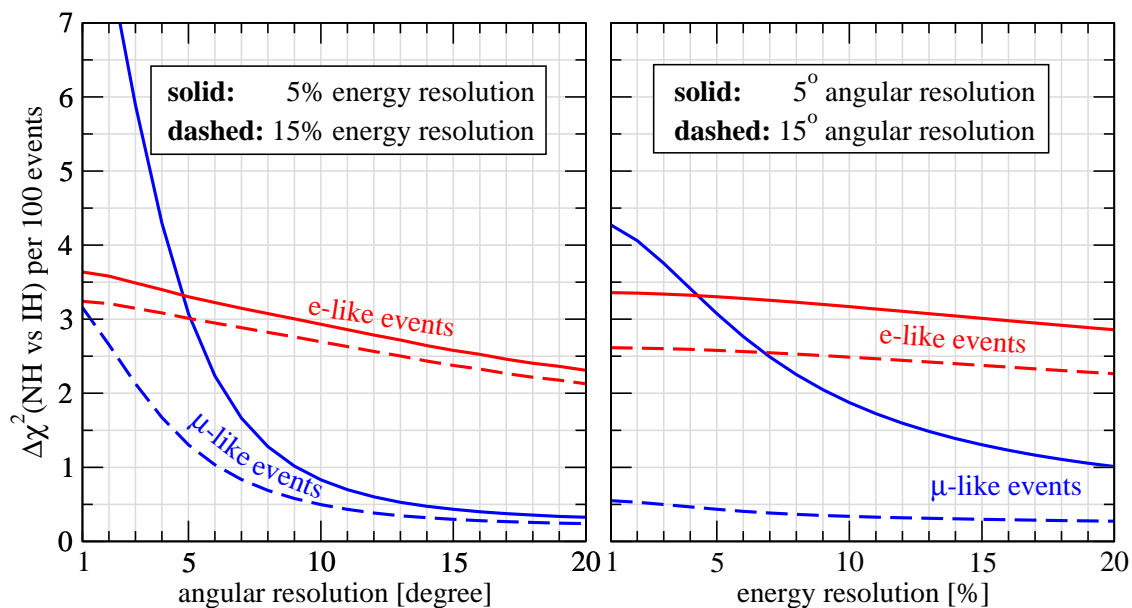
12

Figure 2: $\Delta\chi^2$ between NH and IH per 100 events as defined in Eq. (33) as a function of the angular resolution (left) and energy resolution (right). The oscillation parameters are fixed to $\sin^2 2\theta_{13} = 0.1$, $\sin^2 \theta_{23} = 0.5$, $|\Delta m^2| = 2.4 \times 10^{-3}$ eV^2, and we use 20×20 bins in the intervals 2 GeV $\leq E_\nu \leq$ 10 GeV and $0.1 \leq \cos\theta_n \leq 1$, statistical errors only, and 100% charge identification.

with $\boldsymbol{x}^{\mathrm{IH}} = (\theta_{13}, \theta_{23}, -\Delta m^2)$. The total event number is normalized to 100 according to Eq. (25). It follows from Eq. (29) that for statistical errors only (*i.e.*, $\boldsymbol{\xi} = 0$), the χ^2 is proportional to the total number of events, and hence, our results can be easily scaled for any event number. The scaling in the presence of systematical errors is discussed at the end of this section.

We are aware of the fact that for atmospheric neutrino experiments charge identification is very difficult for electrons. Therefore, most likely only data consisting of μ-like events will be available. Nevertheless, for comparison we show our results also for an e-like event sample of the same size and with the same characteristics as the μ-like data. This will allow us to highlight the advantages or disadvantages of using the μ-like events, and to discuss the different requirements on the experiments.

Let us first explore the impact of energy and angular resolutions. In Fig. 2 we show the $\Delta\chi^2$ between NH and IH as defined in Eq. (33) as a function of the energy resolution and the angular resolution. In agreement with [53] we observe that for μ-like events these resolutions have a dramatic impact on the hierarchy sensitivity. This can be understood from comparing upper and lower panels of Fig. 1. Due to the fast oscillations of the signal, averaging has a rather large effect and leads to a very different final signal. The left panel of Fig. 2 shows that especially for very good angular resolutions $\sigma_{\mathrm{dir}} \lesssim 5°$ and energy resolutions $\sigma_E \simeq 5\%$ a very high sensitivity to the mass hierarchy can be obtained. Even with only 100 events $\Delta\chi^2$-values corresponding to $2 - 3\sigma$ can be achieved, and the sensitivity of μ-like events becomes even better than the one from e-like events.

In contrast, one can see from Fig. 2 that the sensitivity from e-like events is only slightly affected by angular and energy resolutions. The reason for this is that for e-like events the effect does not show such a pronounced oscillatory shape as in the case of μ-like events, but
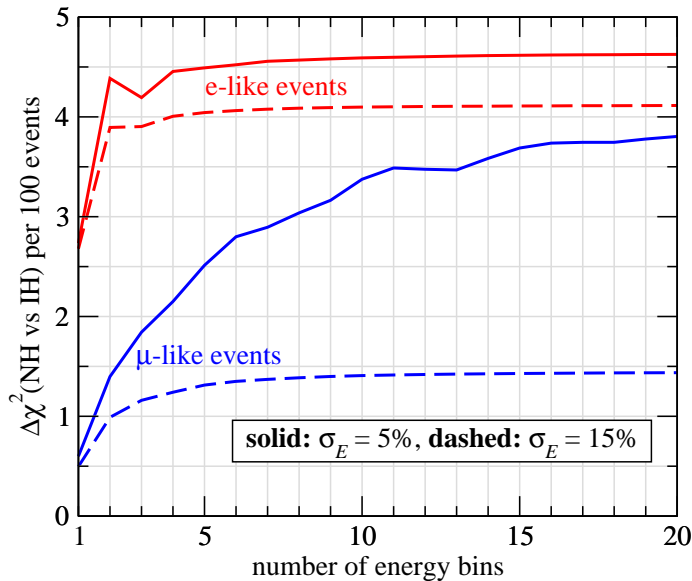
Figure 3: $\Delta\chi^2$ between NH and IH per 100 events as defined in Eq. (33) as a function of the number of energy bins in the interval 2 GeV $\leq E_\nu \leq$ 8 GeV. The oscillation parameters are fixed to $\sin^2 2\theta_{13} = 0.1$, $\sin^2\theta_{23} = 0.5$, $|\Delta m^2| = 2.4 \times 10^{-3}$ eV^2, and we use 10 bins in the interval $0.3 \leq \cos\theta_n \leq 1$, $\sigma_{\rm dir} = 5°$, statistical errors only, and 100% charge identification.

is more similar to the "term A" shown in Fig. 1. (See [41] for a detailed discussion of the hierarchy effect in e-like events in the context of a water-Cherencov detector.) This implies that averaging has a much smaller impact.

We conclude from Fig. 2 that taking into account information on the neutrino energy and direction significantly improves the sensitivity to the neutrino mass hierarchy of μ-like events. This result is confirmed by Fig. 3, where we show the $\Delta\chi^2(\text{NH}; \text{IH})$ as a function of the number of bins in neutrino energy $N_E^{\rm bin}$. The value $N_E^{\rm bin} = 1$ corresponds to only a rate measurement, whereas increasing values of $N_E^{\rm bin}$ imply more spectral information. We observe from that figure that for μ-like events with good energy resolution of $\sigma_E = 5\%$ the spectral information significantly improves the sensitivity to the mass hierarchy. Moving from just a rate measurement to 20 bins in E_ν increases $\Delta\chi^2$ roughly by a factor of 6. For an energy resolution of 15% the optimal $\Delta\chi^2$ is already reached for approximately 8 bins, since for $N_E^{\rm bin} \gtrsim 8$ the energy resolution becomes larger than the bin size, and hence finer binning cannot increase the information. However, also in this case appropriate binning increases $\Delta\chi^2$ approximately by a factor of 3 compared to a pure rate measurement. Furthermore, one finds from Fig. 3 that e-like events are much less sensitive to the number of energy bins, and already for $N_E^{\rm bin} \simeq 2$ the optimal $\Delta\chi^2$ is obtained. This is in agreement with our previous observations in relation with Fig. 2, that e-like events are much less affected by averaging over energy and direction.

In Fig. 4 we show the sensitivity to the mass hierarchy as a function of the charge identification. As expected a bad charge ID has a significant impact on the hierarchy sensitivity since, depending on the hierarchy, the resonant matter effect occurs either for neutrinos or antineutrinos, and hence, distinguishing neutrino from antineutrino events is crucial. A charge ID of 90% leads approximately to a reduction of the $\Delta\chi^2$ of 30% compared to perfect charge ID. For no information on the charge ($f_{\rm ID} = 0.5$) the $\Delta\chi^2$ is reduced roughly by one
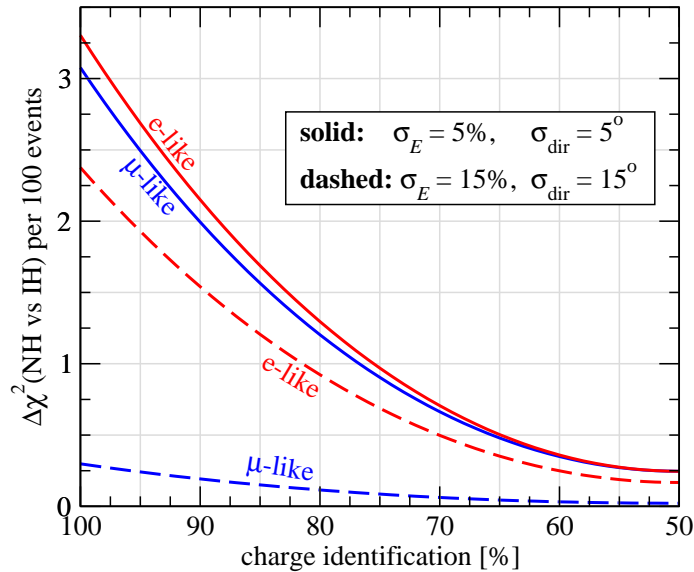
14

Figure 4: $\Delta\chi^2$ between NH and IH per 100 events as defined in Eq. (33) as a function of the charge identification in percent, $100\% \times f_{\text{ID}}$, see Eq. (26). The oscillation parameters are fixed to $\sin^2 2\theta_{13} = 0.1$, $\sin^2\theta_{23} = 0.5$, $|\Delta m^2| = 2.4 \times 10^{-3}$ eV^2, and we use 20×20 bins in the intervals 2 GeV $\leq E_\nu \leq 10$ GeV and $0.1 \leq \cos\theta_n \leq 1$ and statistical errors only.

order of magnitude. This is one reason why in the case of a water Cherencov detector with no possibility to distinguish neutrino from antineutrino events very large exposures of the order of several Mt yrs are necessary to explore the mass hierarchy effect [50].

Finally we investigate the impact of systematical errors and the scaling of the χ^2 with respect to the total number of events. In the left panel of Fig. 5 we show the $\Delta\chi^2$ between NH and IH as a function of the total number of events according to Eq. (25) including systematical uncertainties. The thin solid lines show explicitly for μ-like events that in the case of no systematical errors χ^2 scales linearly with the number of events. Hence, the deviation of the curves in the left panel of Fig. 5 from straight lines with inclination 1 is the manifestation of the systematical errors. We conclude from this figure that—given fixed oscillation parameters as defined in the caption—roughly 4000 events are needed to obtain a 2σ effect for the hierarchy identification using μ-like events with resolutions of $\sigma_E = 15\%$, $\sigma_{\text{dir}} = 15°$. In contrast, using e-like events or high resolution μ-like events, a 2σ sensitivity seems possible already with ~ 200 events.

The impact of the systematics is shown in the right panel, where we display the fractional decrease in $\Delta\chi^2$ by switching on systematical uncertainties. One can read off from that plot that for $N^{\text{tot}} = 100$ the impact is rather small. For the high resolution μ-like sample with $\sigma_E = 5\%$ and $\sigma_{\text{dir}} = 5°$ the $\Delta\chi^2$ is reduced only by 3% due to the systematics; in the other shown cases the decrease in $\Delta\chi^2$ is $\lesssim 12\%$. In this regime the χ^2 is dominated by statistical errors. However, the impact of systematics clearly increases for larger event numbers, leading to a reduction of $\Delta\chi^2$ up to a factor 2 for $\sim 10^4$ events. In Fig. 5 all the systematical uncertainties listed in Tab. 1 are included. We have verified that the uncertainty in the overall normalization has practically no impact, despite the rather large value of 20%. The most relevant systematics are the ones which affect the relative number of neutrino and antineutrino events. In particular, the error on the $\nu/\bar{\nu}$ ratio and the error on the charge ID
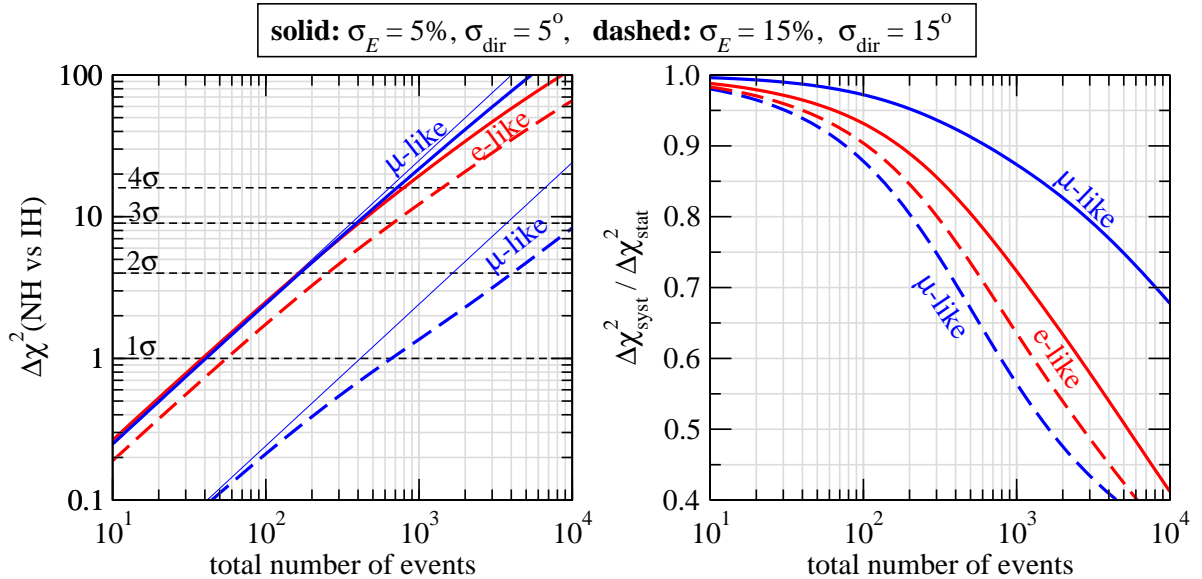
15

Figure 5: We show as a function of the total number of events the $\Delta\chi^2$ between NH and IH as defined in Eq. (33) including systematical uncertainties (left panel), and the ratio between the $\Delta\chi^2(\text{NH};\text{IH})$ including systematical uncertainties and with statistical errors only (right panel). The values for the systematical uncertainties are given in Tab. 1. The thin solid lines in the left panel correspond to statistical errors only (shown only for μ-like events). The oscillation parameters are fixed to $\sin^2 2\theta_{13} = 0.1$, $\sin^2\theta_{23} = 0.5$, $|\Delta m^2| = 2.4 \times 10^{-3}$ eV^2, and we use 20×20 bins in the intervals 2 GeV $\leq E_\nu \leq 10$ GeV and $0.1 \leq \cos\theta_n \leq 1$, and a charge identification of 95%.

parameter f_{ID} are important. Moreover, also the errors on the $\cos\theta_n$ and E_ν shapes are relevant, since we take them to be uncorrelated between neutrino and antineutrino events. In the case of e-like events also the uncertainty on the ν_e/ν_μ flux ratio contributes noticeable, whereas this error has practically no impact for μ-like events.

Let us comment on the relatively small effect of systematics in case of the high resolution μ-like data, visible in the right panel of Fig. 5. This follows from the fact that the discrimination between NH and IH is based on a very characteristic signal (compare Fig. 1), consisting of pronounced structures in the E_ν and $\cos\theta_n$ distributions, which cannot be easily mimicked by the systematic effects. If these structures are washed out to some degree by the averaging implied by worse resolutions, the impact of the systematics is increased, since the effect of changing the hierarchy can be reduced by adjusting the initial fluxes. The same argument applies also in the case of e-like events.

6 Results from the General Fit

Before we are going to present the results of a full fit including all parameters, we define in Tab. 2 three benchmark setups which we will use in the following. We give in the table the experimental characteristics used in the simulation and the χ^2 analysis. All our results in the following are normalized to 200 events for the "true" parameters values. A rough scaling of the results can be performed by using Fig. 5. The difference between the two μ-like event samples S_μ^{high} and S_μ is given by the adopted values for energy and angular resolutions. Setup

setup label	S_μ^{high}	S_μ	S_e
event type	μ-like	μ-like	e-like
total number of events for $\boldsymbol{x}^{\text{true}}$	200	200	200
energy range	2 GeV $\leq E_\nu \leq$ 10 GeV		
Nadir angle range	$0.1 \leq \cos\theta_n \leq 1$		
number of bins in $E_\nu \times \cos\theta_n$	20×20	20×20	20×20
charge identification	95%	95%	80%
systematical errors	included according Tab. 1		
energy resolution σ_E	5%	15%	15%
angular resolution σ_{dir}	$5°$	$15°$	$15°$

Table 2: Definition of example setups.

S_μ^{high} corresponds to a "high resolution" sample with $\sigma_E = 5\%$ and $\sigma_{\text{dir}} = 5°$. These are rather optimistic values which might be achievable only for a very limited number of events by applying appropriate cuts on the muon and on the hadronic event. We discuss setup S_μ^{high} to illustrate the potential of an "optimal" experiment. The values $\sigma_E = 15\%$ and $\sigma_{\text{dir}} = 15°$ adopted for setup S_μ are more realistic and correspond roughly to the numbers given in [52] referring to the MONOLITH detector. Let us add that in a realistic experiment the μ-like data will consist of events of very diverse quality. The accuracy with which neutrino energy and direction can be reconstructed depends strongly on the observed muon energy and on the details of the hadronic event. Therefore, our Setups A and B correspond to ideal cases of well defined energy and direction resolutions, which nevertheless serve as representative examples to illustrate the sensitivity. With setup S_e we show also results for e-like data. Being aware of the fact that charge identification is difficult for electrons we adopt a value of 80%. Although such a number might still be over-optimistic, we include e-like data in our discussion since already with relatively small numbers of events a good sensitivity to the mass hierarchy can be obtained. Moreover, as we have demonstrated in the previous section, for e-like events the accuracies of neutrino energy and direction reconstruction are much less critical than in the case of μ-like data (see Fig. 2).

In the following we discuss the sensitivity of these three example data sets to the mass hierarchy as a function of the assumed true parameter values of θ_{13} and θ_{23}. We present results adopting three different treatments of the oscillation parameters. First we fit the "data" without any additional information on the oscillation parameters, $i.e.$, we minimize $\chi^2(\boldsymbol{x}^{\text{true}}; \boldsymbol{x})$ of Eq. (29) with respect to $\boldsymbol{x}$, where the sign of Δm^2 has opposite values in $\boldsymbol{x}^{\text{true}}$ and $\boldsymbol{x}$. In this case all the parameters have to be determined by the experiment itself. Second, we assume that some external information on the oscillation parameters is available when minimizing with respect to $\boldsymbol{x}$. This information is included by adding a prior function χ^2_{prior} to the χ^2 of Eq. (29), with

$$
\begin{aligned}
\chi^2_{\text{prior}}(\boldsymbol{x}^{\text{true}}; \boldsymbol{x}) \;=\; & \left(\frac{|\Delta m^2| - |\Delta m^2|^{\text{true}}}{\sigma(\Delta m^2)}\right)^2 \\
& + \left(\frac{\sin^2 2\theta_{23} - \sin^2 2\theta_{23}^{\text{true}}}{\sigma(\sin^2 2\theta_{23})}\right)^2 + \left(\frac{\sin^2 2\theta_{13} - \sin^2 2\theta_{13}^{\text{true}}}{\sigma(\sin^2 2\theta_{13})}\right)^2 , \quad (34)
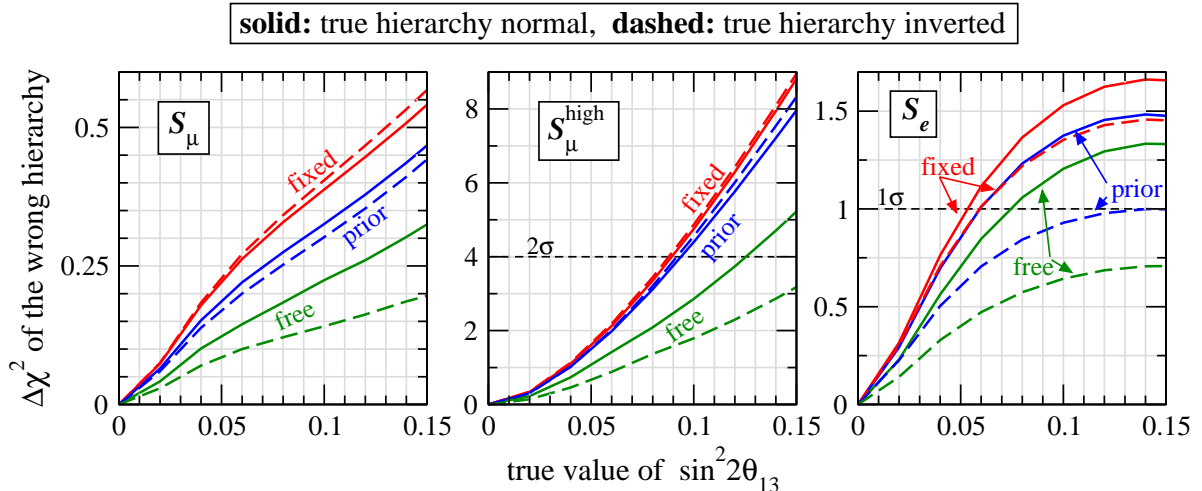\end{aligned}
$$

17

Figure 6: $\Delta\chi^2$ of the wrong hierarchy as a function of the true value of $\sin^2 2\theta_{13}$ for the three data samples defined in Tab. 2, each consisting of 200 events: μ-like data S_μ (left), μ-like data with high energy and angular resolution S_μ^{high} (middle), and e-like data S_e (right). The assumed true parameter values are $|\Delta m^2| = 2.4 \times 10^{-3}$ eV^2, $\sin^2\theta_{23} = 0.5$, and for the solid (dashed) lines the true hierarchy is normal (inverted). For the curves labeled "fixed" the oscillation parameters are fixed to the true values, for the curves labeled "prior" external information is included according to Eq. (35), and for the curves labeled "free" no additional information is assumed.

and we are using the following representative errors at 1σ:

$$\sigma(\Delta m^2) = 0.1\,|\Delta m^2|^{\text{true}}\,, \quad \sigma(\sin^2 2\theta_{23}) = 0.1\,\sin^2 2\theta_{23}^{\text{true}}\,, \quad \sigma(\sin^2 2\theta_{13}) = 0.02\,. \tag{35}$$

These accuracies on $|\Delta m^2|$ and $\sin^2 2\theta_{23}$ can be obtained at the MINOS long-baseline and Super-K atmospheric neutrino experiments, whereas the indicated value for $\sigma(\sin^2 2\theta_{13})$ can be reached in the Double-Chooz reactor experiment [17]. Note that in the way the information on θ_{23} and θ_{13} is included in Eq. (34) we take into account that ν_e (ν_μ) disappearance experiments meassure actually $\sin^2 2\theta_{13}$ ($\sin^2 2\theta_{23}$). In particular, this implies that we include no prior information on the octant of θ_{23}. And third, we also show our results by fixing the oscillation parameters to the true values, *i.e.*, without minimizing the χ^2 with respect to $\boldsymbol{x}$. This corresponds to the ideal case of infinite precision on $|\Delta m^2|$, θ_{23} and θ_{13}.

The results of such analyzes are presented in Figs. 6, 7 and 8. In Fig. 6 we show the $\Delta\chi^2$ of the wrong hierarchy as a function of the true value of $\sin^2 2\theta_{13}$. Clearly, a sizable value of θ_{13} is required since the effect disappears for $\theta_{13} \to 0$. Furthermore, one observes from this figure that external information on the oscillation parameters improves the mass hierarchy sensitivity: Without any external constraints (curves labeled "free") the $\Delta\chi^2$ is significantly reduced compared to fixed parameters. It is interesting to note that for the high resolution sample S_μ^{high} the modest precision implied by Eq. (35) leads already to a sensitivity very close to the one for perfectly known parameters (compare the curves labeled "fixed" and "prior"). Also shown in Fig. 6 is the dependence of the hierarchy sensitivity on the type of the *true* hierarchy (compare solid and dashed curves). One observes that if external information on the oscillation parameters is available for μ-like data, the sensitivity is very similar for a true NH and IH. In contrast, for e-like data the sensitivity is always better for a true NH.

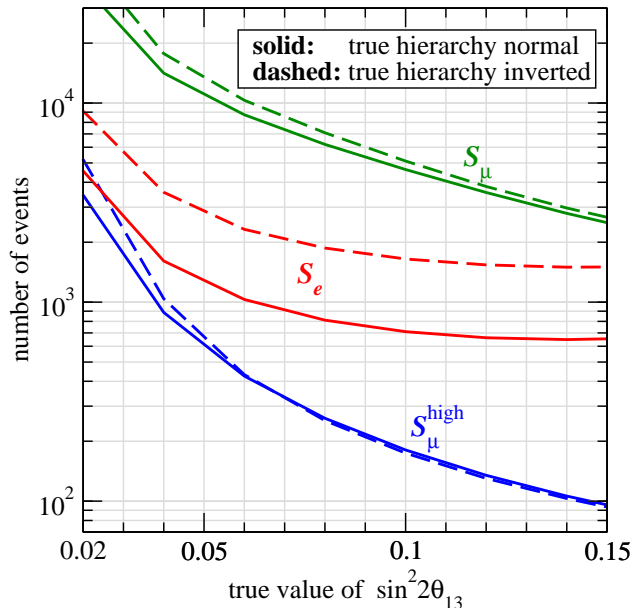In Fig. 7 we answer the question of how many events are needed to exclude the wrong

Figure 7: The number of events needed to exclude the wrong hierarchy at 2σ ($\Delta\chi^2 = 4$) as a function of the true value of $\sin^2 2\theta_{13}$ for the three data samples defined in Tab. 2: μ-like data S_μ, μ-like data with high energy and angular resolution $S_\mu^{\rm high}$, and e-like data S_e. The assumed true parameter values are $|\Delta m^2| = 2.4 \times 10^{-3}$ eV^2, $\sin^2 \theta_{23} = 0.5$, and for the solid (dashed) lines the true hierarchy is normal (inverted). For the oscillation parameters external information is included according to Eq. (35).

hierarchy at 2σ. Considering true values $\sin^2 2\theta_{13} \sim 0.1$ we find that for μ-like data S_μ event numbers of order few$\times 10^3$ are needed, whereas in case of high resolution data $S_\mu^{\rm high}$ already ~ 200 events are sufficient. For e-like data $\mathcal{O}(10^3)$ events are required. For comparison, from Refs. [52,53] we roughly estimate 4 events per kton year in a MONOLITH/INO type detector. Hence, with the proposed detector mass of 30 kton and a 5 year exposure ~ 600 events are obtained. We conclude that for the 15% energy and 15° angular resolutions adopted for S_μ only a very poor sensitivity to the mass hierarchy will be reachable. Therefore, improving the resolutions beyond these values and/or significantly larger exposures seem to be necessary.

Finally we discuss the sensitivity to the mass hierarchy as a function of the true value of $\sin^2 \theta_{23}$. So far we always have assumed maximal mixing $\sin^2 \theta_{23} = 0.5$. As shown in Fig. 8, the ability to identify the true hierarchy depends quite significantly on the true value of θ_{23}, and in general the $\Delta\chi^2$ of the wrong hierarchy increases for increasing $\sin^2 \theta_{23}$. For example, for the data sample S_μ and fixed oscillation parameters, $\Delta\chi^2$ increases by a factor 3 if $\sin^2 \theta_{23}$ is moved from 0.5 to 0.6. However, we note from the left panel of Fig. 8 that for S_μ and $\sin^2 \theta_{23} > 0.5$ the uncertainty on the oscillation parameters has a strong impact on the final sensitivity. The reason is a degeneracy between the octants of θ_{23}: For a true $\theta_{23} > \pi/4$ the data can be fitted better with the wrong hierarchy for $\theta'_{23} \approx \pi/2 - \theta_{23}$. Note that our prior function Eq. (34) is insensitive to the octant of θ_{23}. We have checked that if in addition to the accuracies given in Eq. (35) also the octant of θ_{23} were known, results close to the case of fixed oscillation parameters could be obtained [9]

For the high resolution data $S_\mu^{\rm high}$ shown in the middle panel of Fig. 8 we find that the

---

[9]The possibility of a precision measurement of θ_{23} in an atmospheric neutrino experiment with an iron magnetized detector has been studied recently in [55].
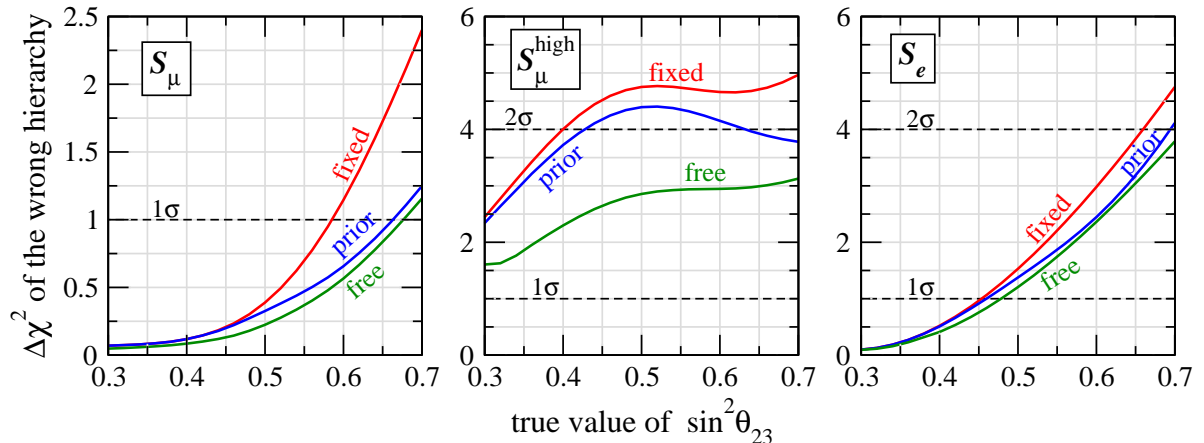
Figure 8: $\Delta\chi^2$ of the wrong hierarchy as a function of the true value of $\sin^2\theta_{23}$ for the three data samples defined in Tab. 2, each consisting of 200 events: μ-like data S_μ (left), μ-like data with high energy and angular resolution $S_\mu^{\rm high}$ (middle), and e-like data S_e (right). The assumed true parameter values are $\sin^2 2\theta_{13} = 0.1$ and $\Delta m^2 = 2.4 \times 10^{-3}$ eV^2 (the true hierarchy is normal). For the curves labeled "fixed" the oscillation parameters are fixed to the true values, for the curves labeled "prior" external information is included according to Eq. (35), and for the curves labeled "free" no additional information is assumed.

maximal sensitivity is reached around maximal mixing $\theta_{23} \approx \pi/4$. As illustrated in Fig. 1, in this case the "term B" contributes significantly to the sensitivity, and the behaviour shown in Fig. 8 follows from an interplay of "term A" (which is increasing with $\sin^2\theta_{23}$) and "term B" (which is proportional to $\sin^2 2\theta_{23}$ and hence has a maximum at $\sin^2\theta_{23} = 0.5$). In contrast, in the case of S_μ the "term B" is suppressed due to the averaging implied by the worse resolutions, and hence, the increase of the sensitivity follows from the $\sin^2\theta_{23}$-dependence of "term A" shown in Eq. (32). Also for e-like events the effect is similar to "term A", and according to Eq. (30) it is proportional to $(r^p \sin^2\theta_{23} - 1)$. As expected, we observe in the right panel of Fig. 8 an increase of the sensitivity with $\sin^2\theta_{23}$, in agreement with Refs. [41, 50].

7 Conclusions

In this work we have reconsidered the possibility to determine the type of the neutrino mass hierarchy by using atmospheric neutrinos in a detector capable to distinguish between neutrino and antineutrino events. For not too small values of the mixing angle θ_{13}, Earth matter effects will lead to different signals in such a detector for a normal or inverted neutrino mass hierarchy. Having in mind magnetized iron calorimeters like MINOS, INO, or perhaps ATLAS, we have performed a χ^2-analysis including realistic neutrino fluxes, detection cross sections, and various systematical uncertainties. We discuss how the performance depends on detector characteristics like energy and direction resolutions or charge miss-identification, and on the systematical uncertainties related to the atmospheric neutrino fluxes. Moreover, we show how the mass hierarchy determination depends on the true values of θ_{13}, θ_{23}, as well as on the true hierarchy. We also compare the potential of μ-like events to a (hypothetical) data sample of e-like events with similar characteristics.

Focusing on the detection of muons, one of our main findings is that the ability to reconstruct the energy and direction of the neutrino is crucial for the mass hierarchy determination. Assuming $\sin^2 2\theta_{13} \simeq 0.1$ and the optimistic values for the neutrino energy and direction reconstruction accuracies of 5% and 5°, respectively, the mass hierarchy can be identified at the 2σ C.L. already with roughly 200 events (sum of neutrino and antineutrino events, including oscillations). In contrast, for less ambitious resolutions of 15% and 15°, of the order of 5000 events are needed. These numbers are based on the detection of muons with a correct charge identification of 95% and an energy threshold of 2 GeV. For illustration we have also considered the potential of using e-like event samples. Assuming energy and direction resolutions of 15% and 15° and a correct charge identification of 80% we find that of order 1000 events are necessary for a 2σ hierarchy determination.

The reason for the relatively high sensitivity which can be achieved using high resolution μ-like events comes from the fact that the difference in the signals for normal and inverted hierarchies shows a characteristic oscillatory behaviour in the neutrino energy, as well as in the Nadir angle. If the energy and direction reconstruction are sufficiently precise to resolve these structures, a statistical analysis using energy as well as directional information (ideally an un-binned likelihood analysis) provides very good sensitivity to the hierarchy. For worse energy and direction reconstruction, these oscillatory structures are averaged out, which leads to a much worse sensitivity. Our results imply that for resolutions of 15% for the neutrino energy and 15° for the neutrino direction, in a MONOLITH/INO-like detector exposures of the order of a few Mton years are required to obtain a reasonable hierarchy sensitivity. However, we stress again that for high quality event samples with more precise reconstruction of the neutrino energy and direction the required exposures are significantly smaller.

References

[1] B. T. Cleveland *et al.*, Astrophys. J. **496** (1998) 505; Y. Fukuda *et al.* [Kamiokande Collaboration], Phys. Rev. Lett. **77** (1996) 1683; J. N. Abdurashitov *et al.* [SAGE Collaboration], J. Exp. Theor. Phys. **95** (2002) 181; T. Kirsten *et al.* [GALLEX and GNO Collaborations], Nucl. Phys. B (Proc. Suppl.) **118** (2003) 33; C. Cattadori *et al.*, Nucl. Phys. B (Proc. Suppl.) **143** (2005) 3.

[2] S. Fukuda *et al.* [Super-Kamiokande Collaboration], Phys. Lett. **B539** (2002) 179; Y. Ashie *et al.*, Phys. Rev. Lett. **93** (2004) 101801.

[3] Y. Ashie *et al.* [Super-Kamiokande Collaboration], Phys. Rev. D **71** (2005) 112005.

[4] Q. R. Ahmad *et al.* [SNO Collaboration], Phys. Rev. Lett. **87** (2001) 071301; *ibid.* **89** (2002) 011301; *ibid.* **89** (2002) 011302; S. N. Ahmed *et al.*, Phys. Rev. Lett. **92** (2004) 181301; B. Aharmim *et al.*, nucl-ex/0502021.

[5] K. Eguchi *et al.* [KamLAND Collaboration], Phys. Rev. Lett. **90** (2003) 021802; T. Araki *et al.*, Phys. Rev. Lett. **94**, 081801 (2005).

[6] E. Aliu *et al.* [K2K Collaboration], Phys. Rev. Lett. **94**, 081802 (2005).

[7] S. T. Petcov, Nucl. Phys. B (Proc. Suppl.) **143** (2005) 159.

[8] B. Pontecorvo, Zh. Eksp. Teor. Fiz. **33** (1957) 549 and **34** (1958) 247; Z. Maki, M. Nakagawa and S. Sakata, Prog. Theor. Phys. **28** (1962) 870.

[9] S. M. Bilenky, J. Hosek and S. T. Petcov, Phys. Lett. **B94** (1980) 495.

[10] J. Schechter and J. W. F. Valle, Phys. Rev. **D22** (1980) 2227; M. Doi *et al.*, Phys. Lett. **B102** (1981) 323.

[11] P. Langacker *et al.*, Nucl. Phys. B **282** (1987) 589.

[12] M. Apollonio *et al.*, Eur. Phys. J. C **27**, 331 (2003); F. Boehm *et al.*, Phys. Rev. Lett. **84** (2000) 3764.

[13] A. Bandyopadhyay *et al.*, Phys. Lett. **B608** (2005) 115; A. Bandyopadhyay *et al.*, 2005, unpublished; see also A. Bandyopadhyay *et al.*, Phys. Lett. **B583** (2004) 134.

[14] J. N. Bahcall, M. C. Gonzalez-Garcia and C. Peña-Garay, JHEP **0408** (2004) 016; M. Maltoni, T. Schwetz, M. A. Tortola and J. W. F. Valle, New J. Phys. **6** (2004) 122; G. L. Fogli, E. Lisi, A. Marrone and A. Palazzo, hep-ph/0506083.

[15] T. Schwetz, hep-ph/0510331.

[16] S. Pascoli and S. T. Petcov, Phys. Lett. **B544** (2002) 239; *ibid.* **B580** (2004) 280.

[17] P. Huber *et al.*, Phys. Rev. **D70** (2004) 073014; Nucl. Phys. B (Proc. Suppl.) **145** (2005) 190 (hep-ph/0412133).

[18] D. Michael *et al.*, Nucl. Phys. B (Proc. Suppl.) **118** (2003) 189.

[19] Y. Itow *et al.*, "The JHF-Kamioka neutrino project," hep-ex/0106019.

[20] V. Martemyanov *et al.*, Phys. Atom. Nucl. **66**, 1934 (2003); H. Minakata *et al.*, Phys. Rev. D **68**, 033017 (2003) [Erratum-ibid. D **70**, 059901 (2004)]; P. Huber *et al.*, Nucl. Phys. B **665** (2003) 487.

[21] K. Anderson *et al.*, hep-ex/0402041.

[22] D. S. Ayres *et al.* [NOvA Collaboration], hep-ex/0503053.

[23] S. Choubey and S.T. Petcov, Phys. Lett **B594** (2004) 333.

[24] J. Beacom and M. Vagins, Phys. Rev. Lett. **93**, 171101 (2004).

[25] A. Bandyopadhyay *et al.*, Phys. Rev. D **72** (2005) 033013.

[26] A. Bandyopadhyay *et al.*, Phys. Rev. **D67** (2003) 113011; H. Minakata *et al.*, hep-ph/0407326.

[27] M. Freund *et al.*, Nucl. Phys. B **578** (2000) 27.

[28] V.D. Barger *et al.*, Phys. Lett. B **485**, 379 (2000); H. Minakata and H. Nunokawa, JHEP **0110**, 001 (2001); P. Huber, M. Lindner and W. Winter, Nucl. Phys. B **645**, 3 (2002), *ibid* **654**, 3 (2003); O. Mena Requejo, S. Palomares-Ruiz and S. Pascoli, hep-ph/0504015.

[29] M. Kachelriess and R. Tomas, hep-ph/0412100; V. Barger, P. Huber and D. Marfatia, Phys. Lett. B **617** (2005) 167.

[30] S. M. Bilenky, S. Pascoli and S. T. Petcov, Phys. Rev. **D64** (2001) 053010; S. Pascoli, S. T. Petcov and W. Rodejohann, Phys. Lett. **B558** (2003) 141; S. Pascoli, S. T. Petcov and T. Schwetz, hep-ph/0505226 (to be published in Nucl. Phys. B).

[31] G. Rajasekaran, AIP Conf. Proc. **721** (2004) 243 (hep-ph/0402246).

[32] N.Y. Ahafonova et al. [MONOLITH Collaboration], proposal LNGS-P26-2000, and `http://castore.mi.infn.it/~monolith/`.

[33] L. Wolfenstein, Phys. Rev. D **17**, 2369 (1978), and *ibid.* D **20**, 2634 (1979).

[34] V. Barger *et al.*, Phys. Rev. D **22**, 2718 (1980).

[35] S. P. Mikheyev and A. Yu. Smirnov, Yad. Fiz. **42**, 1441 (1985).

[36] S. T. Petcov, Phys. Lett. B **434** (1998) 321, (E) *ibid.* B **444** (1998) 584.

[37] S. T. Petcov, Nucl. Phys. B (Proc. Suppl.) **77** (1999) 93, hep-ph/9811205 and hep-ph/9907216; M. V. Chizhov, M. Maris and S. T. Petcov, hep-ph/9810501.

[38] M. V. Chizhov and S.T. Petcov, Phys. Rev. Lett. **83** (1999) 1096, and Phys. Rev. Lett. **85** (2000) 3979.

[39] M. V. Chizhov and S. T. Petcov, Phys. Rev. D **63** (2001) 073003.

[40] J. Bernabéu *et al.*, Phys. Lett. **B531** (2002) 90.

[41] J. Bernabéu, S. Palomares-Ruiz and S. T. Petcov, Nucl. Phys. B **669** (2003) 255.

[42] S. Palomares-Ruiz and S. T. Petcov, Nucl. Phys. B **712** (2005) 392.

[43] G. L. Fogli, E. Lisi, D. Montanino and G. Scioscia, Phys. Rev. D **55**, 4385 (1997).

[44] E. K. Akhmedov *et al.*, Nucl. Phys. B **542**, 3 (1999).

[45] M. C. Bañuls, G. Barenboim and J. Bernabéu, Phys. Lett. B **513**, 391 (2001); J. Bernabéu and S. Palomares-Ruiz, Nucl. Phys. Proc. Suppl. **110**, 339 (2002).

[46] O. L. G. Peres and A. Y. Smirnov, Nucl. Phys. B **680**, 479 (2004).

[47] M. C. González-García and M. Maltoni, Eur. Phys. J. C **26** (2003) 417; M. C. Gonzalez-Garcia, M. Maltoni and A. Y. Smirnov, Phys. Rev. D **70** (2004) 093005.

[48] T. Kajita *et al.* [Super-Kamiokande Collaboration], Talks given *e.g.*, at the Int. Workshop NOON2004, February 11–15, 2004, Tokyo, Japan; NNN05, April 7–9, 2005, Aussois, Savoie, France.

[49] E. Lisi, Talk at the RCCN Workshop on sub-dominant oscillation effects in atmospheric neutrino experiments, December 9–11, 2004, Kashiwa, Japan.

[50] P. Huber, M. Maltoni and T. Schwetz, Phys. Rev. D **71** (2005) 053006.

[51] R. Gandhi *et al.*, hep-ph/0506145.

[52] T. Tabarelli de Fatis, Eur. Phys. J. C **24**, 43 (2002).

[53] D. Indumathi and M. V. N. Murthy, Phys. Rev. D **71** (2005) 013001.

[54] R. Gandhi *et al.*, hep-ph/0411252.

[55] S. Choubey and P. Roy, hep-ph/0509197.

[56] P. I. Krastev and S. T. Petcov, Phys. Lett. B **205** (1988) 84.

[57] S. T. Petcov, Phys. Lett. B **214** (1988) 259.

[58] M. Honda *et al.*, Phys. Rev. D **52**, 4985 (1995); V. Agraval *et al.*, Phys. Rev. D **53**, 1314 (1996); G. Fiorentini, V. A. Naumov and F. L. Villante, Phys. Lett. B **510** (2001) 173.

[59] A. M. Dziewonski and D. L. Anderson, Phys. Earth Planet. Interiors **25** (1981) 297.

[60] F. D. Stacey, *Physics of the Earth, 2nd edition*, John Wiley and Sons, London, 1977.

[61] M. Maris and S. T. Petcov, Phys. Rev. D **56** (1997) 7444.

[62] M. Maris and S. T. Petcov, study pefromed in November-December 1997, unpublished.

[63] M. Honda, T. Kajita, K. Kasahara and S. Midorikawa, Phys. Rev. D **70** (2004) 043008 [astro-ph/0404457]; data tables of atmospheric neutrino fluxes are available at
http://icrr.u-tokyo.ac.jp/~mhonda

[64] M. C. Gonzalez-Garcia and M. Maltoni, Phys. Rev. D **70** (2004) 033010 [hep-ph/0404085].